HHS Public Access

Author manuscript

Cell Rep. Author manuscript; available in PMC 2018 April 10.

Published in final edited form as:

Cell Rep. 2018 January 23; 22(4): 905–918. doi:10.1016/j.celrep.2017.12.097.

Organization of Valence-Encoding and Projection-Defined Neurons in the Basolateral Amygdala

Anna Beyeler[1,2,*], **Chia-Jung Chang**[1,3], **Margaux Silvestre**[1,3], **Clémentine Lévêque**[1], **Praneeth Namburi**[1], **Craig P. Wildes**[1], and **Kay M. Tye**[1,4,5,*]

[1]The Picower Institute for Learning and Memory, Department of Brain and Cognitive Sciences, Massachusetts Institute of Technology, Cambridge, MA 02139, USA

[2]Neurocentre Magendie, INSERM, U1215, University of Bordeaux, 146 rue Léo Saignat, 33077 Bordeaux Cedex, France

Summary

The basolateral amygdala (BLA) mediates associative learning for both fear and reward. Accumulating evidence supports the notion that different BLA projections distinctly alter motivated behavior, including projections to the nucleus accumbens (NAc), medial aspect of the central amygdala (CeM), and ventral hippocampus (vHPC). Although there is consensus regarding the existence of distinct subsets of BLA neurons encoding positive or negative valence, controversy remains regarding the anatomical arrangement of these populations. First, we map the location of more than 1,000 neurons distributed across the BLA and recorded during a Pavlovian discrimination task. Next, we determine the location of projection-defined neurons labeled with retrograde tracers and use CLARITY to reveal the axonal path in 3-dimensional space. Finally, we examine the local influence of each projection-defined populations within the BLA. Understanding the functional and topographical organization of circuits underlying valence assignment could reveal fundamental principles about emotional processing.

Graphical abstract

Basolateral amygdala (BLA) neurons distinctly encode cues predicting rewards or punishments, but how does form give rise to function? Beyeler et al. overlay anatomical projection target, location of neurons in a 3D map, and encoding properties during cue discrimination. The influence on local networks differs across projection-defined BLA populations.

[*]Correspondence: anna.beyeler@inserm.fr (A.B.), kaytye@mit.edu (K.M.T.).
[3]These authors contributed equally
[4]Twitter: @kaymtye
[5]Lead Contact

Supplemental Information: Supplemental Information includes Supplemental Experimental Procedures, six figures, and four movies and can be found with this article online at https://doi.org/10.1016/j.celrep.2017.12.097.

Author Contributions: Conceptualization, K.M.T. and A.B.; Methodology, A.B. and P.N.; Investigation, A.B., M.S., and C.L.; Software, C.-J.C., P.N., M.S., and A.B.; Writing – Original Draft, A.B., K.M.T., and C.-J.C.; Writing – Review & Editing, A.B., C.-J.C., M.S., P.N., C.P.W., and K.M.T.; Funding Acquisition, K.M.T., A.B., and P.N.; Resources, K.M.T. and C.P.W.; Supervision, K.M.T.

Declaration of Interests: The authors declare no competing interests.

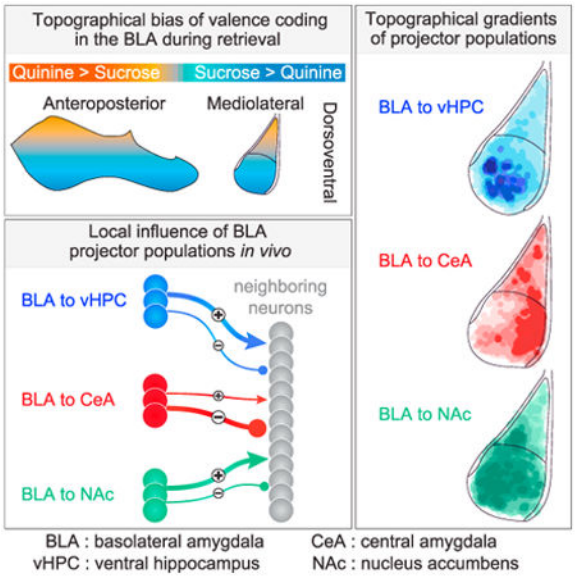

Introduction

The ability to attribute valence to sensory information guides our behavior to approach rewards and avoid danger. How brain circuits achieve this function remains only partially understood. The basolateral amygdala (BLA) complex, including the lateral amygdala (LA) and the basal amygdala (BA), receives dense sensory inputs and is necessary for the acquisition of fear conditioning (Fanselow and Kim, 1994; LeDoux et al., 1990; Maren and Quirk, 2004; Miserendino et al., 1990; Wilensky et al., 1999) and reward associations (Baxter and Murray, 2002; Cador et al., 1989; Cardinal et al., 2002; Tye et al., 2008). Electrophysiological recordings have revealed that BLA neurons respond to cues for both positive and negative valence (Beyeler et al., 2016; Fuster and Uyeda, 1971; Paton et al., 2006; Shabel and Janak, 2009). The valence encoding properties of BLA neurons have been investigated based upon immediate early gene expression (Gore et al., 2015; Redondo et al., 2014) and projection target (Beyeler et al., 2016; Burgos-Robles et al., 2017; Felix-Ortiz et al., 2013, 2016; Namburi et al., 2015). Despite the well-appreciated role of the BLA in valence coding (Janak and Tye, 2015), questions regarding the anatomical organization of neurons encoding positive or negative valence remain unanswered.

Could anatomical organization of BLA neurons contribute to selection of neurons coding for opposite valence? Throughout the brain, motifs of anatomical segregation for functionally defined populations of neurons have been observed, but anatomical intermingled (salt-and-pepper) topographies of functionally distinct neurons have also been reported. Several studies focused on valence encoding in the BLA have reported data that are indirectly suggestive of intermingled populations (Gore et al., 2015; Namburi et al., 2015). Electrophysiological recordings in monkeys revealed intermingled neurons encoding positive and negative valence across the BLA (Zhang et al., 2013).

Antagonistically, it has been proposed that two genetically defined and topographically segregated populations of BLA neurons mediate valence (Kim et al., 2016). Two genetically identified populations were found to correspond to the previously described magnocellular and parvocellular neurons (Alheid, 2003). Neurons expressing the gene Rspo2, coding for R-spon-din 2, located in the anterior BLA correspond to magnocellular neurons, while neurons expressing the Ppp1r1b gene, coding for the protein phosphatase 1 regulatory inhibitor subunit 1B (DARPP-32) are located in the posterior BLA and correspond to parvocellular neurons (Kim et al., 2016; Lein et al., 2007). Optogenetic stimulation of Rspo2 neurons promotes freezing behaviors, and photostimulation of Ppp1r1b neurons supports intra-cranial self-stimulation (Kim et al., 2016). Furthermore, a larger proportion of Rspo2 neurons expresses c-*fos* after an innately aversive experience, and a larger proportion of Ppp1r1b neurons does so after an innately rewarding experience (Kim et al., 2016). However, to meet our criteria for valence encoding, a neuron must (1) respond differentially to stimuli of positive and negative valence and (2) do so independent of stimulus features (Namburi et al., 2016). Given that c-*fos* expression does not reflect phasic inhibitions or allow for temporally precise responses, interpretational discrepancies may be due to differences in the criteria used for valence encoding.

Defining BLA populations by projection target has revealed functional divergences in valence coding (Beyeler et al., 2016; Burgos-Robles et al., 2017; Felix-Ortiz et al., 2013, 2016; Namburi et al., 2015; Stuber et al., 2011; Tye et al., 2011). BLA neurons projecting to the nucleus accumbens (BLA-NAc) were shown to respond preferentially to a reward-predictive cue (Beyeler et al., 2016), and the synaptic strength of the glutamatergic inputs onto these projectors increased after reward conditioning (Namburi et al., 2015). Conversely, BLA neurons projecting to the medial aspect of the central amygdala (BLA-CeM) are preferentially excited to a stimulus predicting an aversive outcome (Beyeler et al., 2016), and the synaptic strength of their inputs increased after fear conditioning (Namburi et al., 2015). Finally, the BLA neurons projecting to the ventral hippocampus (BLA-vHPC) do not express robust preferences for positive or negative valence of conditioned cues, although they mediate innate negative valence as optogenetic activation of BLA terminals in the vHPC increases anxiety-related behaviors (Beyeler et al., 2016; Felix-Ortiz and Tye, 2014; Felix-Ortiz et al., 2013). In summary, the evidence supporting a role for BLA-NAc neurons in positive valence and BLA-CeM neurons in negative valence is three-fold: (1) synaptic changes, (2) optogenetic manipulation, and (3) photo-identified electrophysiological recordings.

To bring evidence to the question of topographical organization of valence coding in the BLA, we mapped the location of 1,000+ neurons acquired in the BLA during a Pavlovian discrimination task. We also performed retrograde and anterograde tracing to locate BLA projection neurons (projectors) and used optogenetic stimulation of these projectors to map their network interactions with the neighboring neurons within the BLA. The locations of positive and negative valence-responsive neurons *in vivo*—and the locations of projection-defined neurons—were both intermingled and distributed across the entire BLA. However, we uncovered the existence of a gradient of valence responses in the dorsoventral axis and a topographical gradient of projectors across the mediolateral dimension of the BLA. Altogether, this study synthesizes projection-defined populations—along with the local

networks they recruit—with classic electrophysiological investigation of valence encoding properties in the BLA.

Results

Preferential Neural Responses to Cues Predicting Reward or Punishment in the BLA

To determine the functional responses of BLA neurons, we previously performed acute single-unit recordings in the BLA of head-fixed mice trained to discriminate between a reward-predictive cue and a cue predicting an aversive outcome (Figure 1A) (Beyeler et al., 2016). Over ~6 days, mice learned the associations of one auditory cue with the delivery of a drop of sucrose solution (sucrose predictive conditioned stimulus, CS-S), measured by anticipatory licking, and a second auditory cue with the delivery of a drop of the bitter substance (quinine predictive conditioned stimulus, CS-Q), which suppressed licks. We recorded BLA neurons during the discrimination task and located each recording site by coating the silicon probe with fluorescent beads.

In light of studies describing topography of valence coding, we performed analyses on these data, integrating the valence coding properties and the histologically determined location of the neurons (Figure 1B) in the anteroposterior (AP), mediolateral (ML), and dorsoventral (DV) dimensions of the BLA. Based on normalized responses of each unit to the CS onset (before sucrose or quinine delivery), BLA neurons overall had a stronger response to the sucrose-predictive cue (CS-S) compared to the quinine-predictive cue (CS-Q). The Z score in response to the CS-S is significantly higher when averaged across all BLA units (Figure 1C, right inset). The bias toward the sucrose cue is present at most coordinates, as shown by the positive differential Z score between the CS-S and the CS-Q at most AP, ML, and DV coordinates (Figure 1C). In the DV dimension, only the ventral section showed a consistent bias toward the positive cue (Figure 1C, right panel).

Next, we examined the responses to the unconditioned stimuli (US; sucrose and quinine). To assess the neural responses to quinine, in this study, we restricted our analyses to sessions containing at least 5 quinine consumptions (error trials, because CS-Q is typically a no-go cue) (Figure 1D). We recorded 681 units during quinine consumptions (n = 44 sessions, 14 mice) and histologically located them along the AP, ML, and DV axes of the BLA (Figure 1E). In contrast to the bias for the CS-S over the CS-Q, when examining the responses to the US consumption, BLA neurons tended to be more responsive to quinine consumptions (Figure 1E, right inset) in a consistent manner across the AP, ML, and DV axes of the BLA (Figure 1F).

This suggests that the representations of CSs are distinct from the representations of the USs and may represent not only valence coding properties but also information including action selection (go or no-go) and prediction error (correct or error) (Grabenhorst et al., 2012; Baxter et al., 2000; Schoenbaum et al., 1999).

Preference for Excitatory Responses to a Sucrose-Predictive Cue in BA Neurons

One possible explanation for discrepancies between studies using immediate early gene expression versus electrophysiological recordings as a readout for neural activity is the

differences in the information captured by each approach. Immediate early gene expression is thought to only reflect neuronal activation, and stimulus-driven inhibitions would not be reflected. In contrast, electrophysiological recordings can reflect both excitatory and inhibitory responses (time-locked phasic increases or decreases in firing rate upon stimulus presentation), as well as graded responses reflecting relative magnitude (often displayed as Z score).

To address this, we separated the excitatory and inhibitory responses to the sucrose and quinine cues across the three dimensions of the BLA (Figure 2A). Both excitations and inhibitions were observed across the entire BLA, with excitatory responses to the CSs (sucrose and/or quinine) overrepresented in the posterior, lateral, and dorsal BLA, compared to inhibitory responses (Figure 2B). Parsing the excitatory responses to the CS-S and CS-Q revealed a larger proportion of neurons excited to the sucrose cue in the ventral BLA compared to neurons excited to the quinine cue (Figure 2C). We observed the opposite trend for inhibitory responses (Figure 2D). We also noted a different distribution between the ML axis, with more units inhibited to the CS-S around 3 mm lateral from bregma (Figure 2D). The proportion of units with a stronger response to the CS-S than the CS-Q matched the trend of the average Z score for all neurons at these coordinates to be larger for the CS-S than the CS-Q (Figure S1B), suggesting that the effect is supported by a higher response for a large proportion of units, rather than a few neurons dramatically increasing their response.

Projectors are Enriched in Different Subregions of the BLA

To test whether the valence biases we observed are supported by a topographical organization of projector populations, previously described as preferentially encoding positive or negative valence (Beyeler et al., 2016), we injected retrograde tracers in downstream targets of the BLA (vHPC, CeM, and NAc) (Figures 3A and S2). After sectioning the mouse brain in coronal slices and confirming the location of the tracer injections (Figures S2D–S2I), the BLA was imaged in at least six AP coordinates and the projection neurons containing fluorescent tracers were counted (Figures 3B and S3). Because we could not determine the efficiency of the third tracer (fast blue), we restricted our analysis to the injections of cholera toxin subunit B conjugated with Alexa Fluor 555 or 647 (CTB 555 or CTB 647) in two downstream regions (Figures 3D–3I), counterbalanced across regions (Figure S2B). Neurons from each of the three BLA projector populations were present throughout the entire amygdala; however, we did observe hotspots or subregions with a higher relative density of projector populations (Figures 3 and S3).

To visualize the gradients of projector locations, and to determine how consistent these patterns were across animals, we computed each population's local density (50 μm radius cylinder in 50 μm slices) (Figure S4A), color coded the density, and overlaid it across all neurons, depending on their AP coordinates (anterior, intermediate, and posterior slices) (Figures 3D–3I and S4A–S4C). The BLA-vHPC projectors were densest in the posterior-ventral BLA but were equally distributed along the lateral, medial, and dorsal axes of the BLA complex (Figure 3E). The BLA-CeM projectors were preferentially located in dorsal BLA (LA), in the anterior and intermediate sections, and they were densest in the lateral BA in the posterior sections (Figures 3F and 3G). As for the BLA-NAc population, the density

was greatest in the medial part of the BA (Figures 3H and 3I) across the entire AP axis (Figure S4C).

Finally, we sought to view the 3-dimensional BLA circuitry in the intact brain by expressing a cre-dependent fluorophore into the BLA and the retrogradely traveling canine adenovirus 2 (CAV_2-cre), which allowed for the expression of cre recombinase (Kremer et al., 2000). Using CLARITY (Chung et al., 2013), a whole-brain clearing method, we visualized each projection within the intact brain (Figures S4D–S4I). BLA-NAc neurons and their axonal path are imaged in Movie S1, starting with a sagittal view; BLA-CeM neurons are imaged in Movie S2; and these populations (BLA-NAc and BLA-CeM) can be seen together in Movie S3. In Movie S3, we can observe the preferential location of BLA-NAc projectors in the media BLA (green) and of the BLA-central amygdala (CeA) projectors in the more lateral part of the BLA (pink; see movie orientation in Figure S4F). In Movie S4, we reveal BLA-vHPC neurons (Figure S4G). The divergent paths for populations targeting the same general region (vHPC, CeA, and NAc) suggest distinct chemical signals to guide axon growth during development, raising speculation regarding functionally relevant heterogeneity within a projection defined solely by source and target.

To test whether single neurons project to the three downstream regions, we analyzed mice with retrograde tracer injections in the three downstream targets and with counterbalanced dye locations (CTB 555, CTB 647, and fast blue, FB; n = 5 mice) (Figure 4). Because we could not determine the efficiency of fast blue or identify its mechanism of transport, we decided to restrict our analysis the injections of CTB 555 and CTB 647 (Figures S3D and S3E).

However, we refrain from drawing conclusions regarding the proportion of neurons in the BLA that send collaterals to other targets, given that retrograde labeling suffers from undersampling errors because (1) tracers have limited efficiency in retrograde transport and (2) injections are performed to prioritize specificity over coverage of the target region (injections leaking outside of the target region are excluded, while injections that do not spread to cover the entire target region are included). So in all cases, we are only labeling a subset of the projectors, and our estimates are conservative (false negatives > false positives). This retrograde-based investigation of collateralization complements our previous anterograde-based investigation of collateralization published in Figure S3 of Beyeler et al. (2016).

BLA Projectors Locally Influence the Firing of Neighboring Neurons *In Vivo*

To characterize the influence of BLA projectors on the neighboring cells within the BLA, we expressed channelrhodopsin-2 (ChR2) specifically in each projector population (BLA-NAc, BLA-CeA, and BLA-vHPC) using a cre-dependent dual-virus approach (Figure 5A) (Beyeler et al., 2016). Although the CAV_2-cre viral injections were aimed at the CeM using the same coordinates as for the retrograde tracers, we could not rule out the possibility of some leak into the centrolateral amygdala and thus refer to this population as BLA-CeA for this portion of the experiments to be conservative. At least six weeks after viral vector delivery, we used 10 ms pulses of blue light (15 mW, 1,910 mW/mm^2) to photostimulate the projectors while recording the neural activity of neighboring cells *in vivo* (Figure 5A). For

each projector population, we found cells that were phototagged and expressing ChR2 (displaying an excitatory response to the light stimulation with a short latency), cells that were polysynaptically excited by the photostimulation (longer photoresponse latency, which we term network-excited), and cells that were inhibited by the light stimulation (network-inhibited) (Figure 5B). The kinetics and amplitudes of the population photores-ponses from each category (phototagged, network-excited, and network-inhibited) were similar after photostimulation of each population (BLA-vHPC, BLA-CeA, and BLA-vHPC) (Figures 5C–5E). Across 5 mice expressing ChR2 in BLA-vHPC projectors, 46% of neurons were photoresponsive (192/421). Of the 7 mice expressing ChR2 in BLA-CeA projectors, 38% were photoresponsive (211/559), and 21% (138/646) were photoresponsive units in 9 mice expressing ChR2 in BLA-NAc projectors (Figure 5F).

One striking observation was that the proportion of network-excited or network-inhibited neurons differed across the three experimental groups (Figures 5F–5H). Because the number of photoresponsive neurons through activation of the projectors. depends on the number of phototagged neurons, we normalized the proportion of polysynaptically photoexcited (network-excited) and photoinhibited (network-inhibited) neurons to the number of phototagged (ChR2+) units (Figure 5G). If we normalize how many units are network-excited or network inhibited to the number of phototagged units, more than twice as many neurons are network-excited (231%) as are photo-tagged for BLA-vHPC (100% = 39 cells), which also network inhibits 162%. In contrast, BLA-CeA excites 197% and inhibits more than three times the number of phototagged units (342%). Finally, BLA-NAc excites and inhibits only a slightly higher percentage of units than were phototagged (142% and 121%, respectively) (Figure 5G).

To assess the balance of network-driven excitation and inhibition recruited by each projector population, we computed the proportion of network-excited and network-inhibited neurons in response to photostimulation of the projectors (Figure 5H). We found that BLA-CeA projectors inhibited a significantly greater proportion of neighboring neurons compared to BLA-vHPC and BLA-NAc projectors (binomial test, ***$p < 0.001$), which had greater proportions of network-excited units in response to projector activation.

This suggests that the connectivity of BLA neurons is related to the projection target and these projections interact locally through functionally distinct microcircuits. BLA-CeA projectors are more prone to suppressing other outputs, while BLA-vHPC and BLA-NAc projectors are more prone to facilitating other outputs.

Valence Coding of BLA Projectors Microcircuit *In Vivo*

To test whether the cells connected to one projector population belong to the same functional microcircuit, we compared the changes in firing rates of the identified projectors (phototagged neurons) in response to the cues associated to sucrose (CS-S) or quinine (CS-Q) with the changes in firing rates of the units recruited by the identified projectors (polysynaptically network-excited or network-inhibited). Despite the qualitatively similar response profiles of the population Z score time course for network-excited and network-inhibited neurons (Figures 6A–6C), differences in responses to CS onset and offset were observed between projector and network populations (Figures 6D–6G, S5, and S6). BLA-

CeA phototagged and network-excited units had an excitatory response to CS onset (CS-S and CS-Q) and to the CS-S offset compared to the BLA-CeA network-inhibited units, which were inhibited by CS onset and CS-S offset (Kruskal-Wallis test, $p < 0.001$, for Figures 6D, 6E, and 6G, and Dunn's post hoc test, ***$p < 0.001$, for all comparisons, except for comparison of BLA-CeA network-excited and network-inhibited in response to the CS-Q onset, where *$p < 0.05$).

When comparing the valence response of the phototagged, network-excited, and network-inhibited units of the three networks, only the network-inhibited units showed differential response profiles to the CS-S onset, with the BLA-vHPC and BLA-NAc network-inhibited units being excited to the CS-S while BLA-CeA network-inhibited units are inhibited to the CS-S (Dunn's post hoc test, ***$p < 0.001$ and *$p < 0.05$, for both comparisons) (Figure 6D). Only phototagged units showed differential response to the CS-Q onset, with the BLA-vHPC and BLA-CeA having a larger response to the CS-Q onset compared to the BLA-NAc projectors (Dunn's post hoc test, BLA-vHPC versus BLA-NAc, *$p < 0.05$, and BLA-CeA versus BLA-NAc, ***$p < 0.001$).

Similar to BLA-vHPC phototagged units, the BLA-vHPC network-excited population (Figure 6A, black) showed phasic excitations in response to both the onset and the offset of cues, regardless of whether they predicted sucrose or quinine (Figures 6A and S5). Although the BLA-vHPC network-inhibited population showed similar excitation in response to the CS-S onset, the excitations to CS-S and CS-Q offsets were significantly lower in amplitude than for the BLA-vHPC phototagged population (Kruskal-Wallis test, $p < 0.001$, and Dunn's post hoc test, photo-tagged versus network-inhibited, *$p < 0.05$, for CS-S offset and, **$p < 0.01$, for CS-Q offset, for Figures 6F and 6G).

Discussion

Preferential Coding of Predictive Cues of Positive Valence in the BA

In line with previous electrophysiological studies, we observed that the distribution of positive and negative valence coding neurons, as described by their preferential response to cues predicting a positive or a negative outcome, was intermingled in the BLA (Zhang et al., 2013). However, acute *in vivo* recordings in mice allow us to sample a larger number of neurons, which permitted us to unravel a valence coding bias across the DV axis of the BLA. The BA had a stronger response to the sucrose-predictive cue compared to the LA in terms of average response of all neurons; in terms of numbers of units excited to the CS-S, which were significantly more ventral than units excited to the CS-Q; and finally, in terms of number of neurons inhibited to the CS-Q, which tended to be more ventral.

Similar Valence Response to Predictive Cues along the AP Axis of the BLA

In contradiction to a previous study describing two genetically defined populations segregated along the AP axis of the BLA in the context of valence (Kim et al., 2016), we were unable to detect a topographical gradient across the AP axis for neurons encoding positive and negative valence of learned cues or innate outcomes. One possible explanation is that electro-physiological recordings reveal both excitatory and inhibitory responses,

which immediate early genes may not reflect. Another experimental difference is that we quantified responses of individual neurons to stimuli of both positive and negative valence to meet criteria for valence encoding (Namburi et al., 2016).

One caveat is that we did not record in the most posterior section of the BLA (from −2.46 to −2.80 mm from bregma). However, our recordings included parts of the BLA containing a large number of neurons located in the region reported to contain mainly parvocellular neurons (more than −2.18 mm from bregma; 99 of 1,626 neurons in our dataset, 6%). Moreover, the heterogeneity we observed is consistent with the expression of *c-fos* in both the anterior and the posterior BLA, with the differential proportion depending on the valence of the experience (Gore et al., 2015; Kim et al., 2016).

Anatomical definition of the sections of the BLA may also explain discrepancies among studies. Here, we defined the BLA from the Paxinos and Franklin (2004) mouse atlas, including the posterior medial BLA (BLP) and excluding the anterior and posterior parts of the basomedial amygdaloid nucleus (BMA and BMP, respectively).

Topographical Gradients of BLA Projectors

Consistent with the intermingling of neurons with different valence coding properties, we found that BLA neurons projecting to the vHPC, CeM, and NAc are present in the entire BLA. However, we identified preferential locations of the three projector populations, which are correlated with the opposing valence biases of the BLA-NAc and BLA-CeA projector populations (Beyeler et al., 2016). In line with the preference of the BLA-CeA population to code for negative valence, in this study, we found a higher density of BLA-CeA units in the dorsal section of the BLA across the entire AP axis and more units excited by the cue predicting an aversive outcome in the dorsal BLA. Consistently, we found that BLA-NAc projectors are more concentrated in the ventral BLA and that BLA units in the ventral BLA are preferentially excited by the reward-predictive cue.

However, the three projector populations we studied are part of a more complex BLA network containing many other anatomically defined populations, including the neurons projecting to the medial prefrontal cortex (BLA-mPFC) and the ones projecting to the bed nucleus of the stria terminalis (BLA-BNST) or to the insular cortex (BLA-IC). Including the topography of these other populations will drastically increase the complexity of the valence mapping in the BLA but might also bring evidence regarding our recordings of non-specific units across the entire BLA.

Further underscoring the complexity of the BLA from the perspective of overlaying functional role and projection target is that even within source-to-target-defined projections, parallel paths may be taken, as revealed with CLARITY (Movies S1, S2, S3, and S4). Our results are in agreement with prior evidence that projections are heterogeneous in terms of the location and/or cell type they contact within the downstream target, because anterior BLA-NAc projectors preferentially target the anterolateral NAc, whereas the posterior BLA-NAc neurons preferentially target the posteromedial NAc (Krettek and Price, 1978). Further investigation of the macrostructural organization of amygdalar circuits is required to determine the significance of these parallel pathways.

Collateralization of BLA Projector Populations

Collateralization is a defining feature of projection neurons, and synapses of one projection-defined population onto different downstream regions might support diverse behavioral effects. Stimulating the cell bodies of a population of BLA projectors might have a different impact on behavior compared to the selective stimulation of the terminals in one downstream region. In previous studies, we showed that BLA-vHPC, BLA-CeA, and BLA-NAc populations collateralize to one another's downstream targets, with up to 50% of the main downstream region's relative fluorescence found in collateral regions (Beyeler et al., 2016). Again, including collateralization to other regions such as the mPFC, BNST, or IC would increase the heterogeneity of defining features of each BLA neuron. In addition, known and unstudied genetic markers may correspond to defining features that map onto the collateralization pattern and valence coding properties.

Projection-Defined Components of Amygdala Microcircuits

Although a number of studies have investigated the functional role of BLA projections using projection-specific optogenetic manipulations in behavior, this approach is not physiological. Furthermore, we have drawn our conclusions based on the assumption that these projections are working independently, or with similar local network effects. Here, we show that the impact of activating projection-defined populations of BLA neurons recruits different extended microcircuits (which are greater than the number of projection-defined cells activated). The differences in the microcircuits recruited reveal a richer landscape for network interactions within the BLA.

The BLA-vHPC projector population (n = 39), recruits more network-excited than network-inhibited neurons (n = 90 and n = 63, respectively) within our sample, and the network-excited neurons are robustly excited in response to the onset and offset of both the CS-S and the CS-Q (Figure 6A). The BLA-vHPC projector population recruits a network 392% the size of itself. This is consistent with the notion that activation of BLA-vHPC neurons can increase anxiety-related behavior in the absence of conditioning (Felix-Ortiz et al., 2013), because activation of these neurons may heighten responsiveness to US in a state of increased arousal and vigilance. In contrast, the BLA-vHPC network-inhibited population (n = 63) only shows a robust response to the CS-S onset, with smaller responses to the CS-S offset or the CS-Q onset or offset relative to the network-excited population (Figure 6). Thus, BLA-vHPC neurons facilitate activity in neurons that are more generally stimulus responsive and suppress activity in neurons that are more selective to a reward-predictive cue.

In contrast, our data suggest a more complex role for the BLA-CeA population than may have been previously appreciated. This may synthesize apparently conflicting studies reporting the role of the CeA in freezing and avoidance (Ciocchi et al., 2010; Davis and Shi, 1999; Duvarci and Pare, 2014; Fadok et al., 2017; Goosens and Maren, 2001; Haubensak et al., 2010; Jimenez and Maren, 2009; Li et al., 2013; Maren and Quirk, 2004; Penzo et al., 2014; Sanford et al., 2017; Viviani et al., 2011) versus appetitive or anxiolytic behaviors (Corbit and Balleine, 2005; Hall et al., 2001; Han et al., 2017; Holland and Gallagher, 2003; Kim et al., 2017; Tye et al., 2011).

BLA-CeA (primarily BLA-CeM) neurons are well positioned to play a role in state-dependent action selection, because the neurons that are network-excited and network-inhibited have qualitatively opposing response profiles (Figure 6). Furthermore, BLA-CeA neurons inhibit significantly greater proportions of neurons than they excite (Figures 5F and 5G), consistent with a role for gating action selection. Another defining feature of BLA-CeA projectors is that the network-excited population is qualitatively more similar to the projectors than the network-inhibited population (Figures 6D–6G). Although future experiments are required to elucidate the identity and function of BLA-CeA network-inhibited cells, we speculate that these neurons (representing 539% of the phototagged population) are diverse in the projection target and behaviors they evoke. In contrast, BLA-vHPC and BLA-NAc photoidentified neurons showed more qualitatively similar responses to their respective network-inhibited populations (Figures 6D–6G).

Why would a population facilitate neurons with opposing responses but inhibit neurons with similar response profiles? Neurons with similar responses to stimuli do not need to all participate in a similar manner in driving behavior—and suppressing different behavioral actions may be precisely what neurons that select a specific action must do.

BLA-NAc neurons show relatively balanced proportions of neurons that are network-excited and network-inhibited (Figure 5). Furthermore, these in-network populations show remarkably congruent response profiles to the BLA-NAc neurons and one another in terms of selective excitatory responses to the CS-S onset (Figures 6C, 6D, 6F and 6G). The accumulation of evidence surrounding the BLA-NAc projection has consistently supported the role of this projection in mediating positive valence and appetitive behavior (Beyeler et al., 2016; Britt et al., 2012; Namburi et al., 2015; Ramirez et al., 2015; Stuber et al., 2011).

In contrast to the BLA-CeA neurons, the BLA-NAc neurons have relatively modest impact on the local circuitry (modulating activity of only 263% of the phototagged population). We speculate that the role of this projection across studies and conditions may be related to the relatively restricted network that this population recruits and that this may be flexible depending on the internal state signaled by sources such as the paraventricular thalamic input (Do-Monte et al., 2017; Haight et al., 2017; Livneh et al., 2017). Altogether, these findings are consistent with evidence that reward- and threat-predicting cues recruit distinct subsets of BLA neurons (Lee et al., 2017).

In conclusion, the BLA, which is often deemed primitive due to its lack of a laminar structure, has an intricate anatomical architecture. Whether its function relies on the layers of topographical gradients or functions despite this vestige of disorganization is yet unknown. The existing information begs for further investigation of the microcircuit interactions on a synaptic level, as well as the changes across different behavioral states. Both recording and immediate early gene readouts for neural activity and identification of both the genetic and the anatomical features of neuronal populations will be important for a comprehensive understanding of amygdala circuitry.

Experimental Procedures

See the Supplemental Information for detailed procedures.

Animal Care and Surgery

All procedures for handling animals were in accordance with the guidelines from NIH and with approval from the Massachusetts Institute of Technology (MIT) Committee on Animal Care (CAC). Adult wild-type male C57BL/6 mice were maintained with a reverse 12 hr light/dark cycle with *ad libitum* food and water, except during behavioral training and electrophysiological recordings. All surgeries were performed on mice aged 8–12 weeks (Jackson Laboratory, Bar Harbor, ME) and conducted under aseptic conditions using a digital small animal stereotaxic instrument (David Kopf Instruments, Tujunga, CA). For surgery, mice were anesthetized in a sealed box containing gaseous isoflurane (5%) and maintained under anesthesia in the stereotaxic frame (1.5%–2.0% isoflurane) for the entire surgery while their body temperatures were kept ~36°C with a heating pad. After surgery, the body temperature was maintained using an infrared heat lamp until the mice fully recovered from anesthesia.

In Vivo Electrophysiology

A subset of these data was previously analyzed in Beyeler et al. (2016). For additional methodology, refer to this publication. To express ChR2 fused to enhanced yellow fluorescent protein (eYFP) only in neurons of the BLA projecting to a specific downstream target, AAV_5-EF1 α-DIO-ChR2-eYFP was injected into the BLA and CAV_2 carrying cre recombinase (CAV_2-cre) or a 1:1 mixture of CAV_2-cre and HSV-hEF1α-mCh-IRES-cre was injected into the vHPC, the CeM, or the NAc (see Figure S2 for coordinates). Approximately 11 weeks after viral surgery, mice were head-fixed, and two auditory cues were played in anticipation of deliveries of either sucrose or quinine solutions (1 and 8 kHz, counterbalanced between animals). During the first 2 days, only one cue was played, and 500 ms after the onset of the auditory cue, a drop of sucrose solution was delivered. After mice acquired this association, indicated by anticipatory licking, we introduced the second auditory cue paired with a delivery of 1 mM quinine solution. After ~6 days of training, mice reached the learning criterion (>70 success rate for each association), and we recorded neural activity in the BLA using the silicon optrode (A1×16-Poly2-5mm-50 s-177, Neuronexus) coated with red fluorescent latex microspheres to locate the recording site. Recordings were performed using a RZ5D TDT system while presenting at least 30 sucrose and 30 quinine interleaved trials. Following completion of the task, a photo-identification session using a 473 nm laser was conducted (15 mW, 1 Hz, and 10 ms). An offline sorter (Plexon) was used for sorting single units, and neural responses of every unit in response to cues and light stimulations were analyzed using MATLAB software.

Retrograde Tracing of BLA Projector Populations and Histology

To label BLA-vHPC, BLA-CeM, or BLA-NAc projectors, we injected three fluorescent tracers in each projection target (Figure S2A). CTB 555 or CTB 647 or fast blue (FB) were used. One week after the surgery, the mice were deeply anesthetized and transcardially perfused with ice-cold Ringer's solution, followed by ice-cold 4% paraformaldehyde (PFA)

in PBS (pH 7.3). Extracted brains were fixed in 4% PFA overnight and then equilibrated in 30% sucrose in PBS. Then, 50 μm thick coronal sections were sliced using a sliding microtome and stored in PBS at 4°C. Sections were mounted on microscope slides with polyvinyl alcohol (PVA)-DABCO. Images were acquired with an Olympus FV1000 confocal laser scanning microscope. BLA projectors containing fluorescent tracers were counted and located using Imaris software (Bitplane) and then analyzed using MATLAB software, in which the coordinates of each spot were normalized to the most dorsal point of the BLA. The density of projection-defined neurons in the BLA was calculated and represented in heatmaps (Figures 3C, 3E, and 3G). To quantify the location biases observed on the heatmaps, the BLA was split in three subregions: LA, medial BA, and lateral BA.

Anterograde Tracing of BLA Projector Populations with CLARITY

AAV_5-EF1α-DIO-eYFP was injected into the BLA and CAV_2-cre, or a 1:1 mixture of CAV_2-cre and HSV-hEF1α-mCh-IRES-cre was injected into the vHPC, CeM, or vHPC (see Figure S2A for coordinates). To express eYFP only in the BLA-NAc projector population and mCherry in BLA-CeA projectors, we injected HSV-hEF1α-flp in the NAc, CAV_2-cre in the CeM, and a mixture (1:1) of AAV_5-EF1α-fDIO-eYFP and AAV_5-EF1α-cDIO-mCh in the BLA. The clearing protocol was adapted from Chung et al. (2013). Confocal fluorescence images were acquired from cleared half-brains using a Leica TCS SP8 white laser confocal scanning microscope.

Statistical Analysis

The thresholds for significance were placed at $*p < 0.05$, $**p < 0.01$, and $***p < 0.001$. All data are shown as mean and SEM unless stated otherwise. Paired Student's t test, repeated-measure ANOVA, Wilcoxon signed rank-sum test (paired), Kruskal-Wallis ANOVA followed by a Dunn's post hoc test, and binomial test were performed using GraphPad Prism 6 or MATLAB. The p values were corrected for multiple comparisons.

Supplementary Material

Refer to Web version on PubMed Central for supplementary material.

Acknowledgments

We thank the entire K.M.T. laboratory for helpful discussion. We thank K. Chung and his lab for advice regarding CLARITY. We thank E.J. Kremer for providing the CAV_2-cre vector, R.Neve for the HSV vectors, and the University of North Carolina (UNC) vector core for the AAV_5 vectors. K.M.T. is a New York Stem Cell Foundation Robertson Investigator and McKnight Scholar, and this work was supported by funding from the JPB Foundation, PIIF, PNDRF, JFDP, Whitehall Foundation, Klingenstein Foundation, NARSAD, Alfred P. Sloan Foundation, New York Stem Cell Foundation, NIH grant R01-MH102441 (NIMH), and NIH Director's New Innovator Award DP2-DK-102256 (NIDDK). A.B. was supported by a fellowship from the Swiss National Science Foundation and NARSAD. P.N. was supported by Singleton, Leventhal, and Whitaker fellowships.

References

Alheid GF. Extended amygdala and basal forebrain. Ann N Y Acad Sci. 2003; 985:185–205. [PubMed: 12724159]

Baxter MG, Murray EA. The amygdala and reward. Nat Rev Neurosci. 2002; 3:563–573. [PubMed: 12094212]

Baxter MG, Parker A, Lindner CCC, Izquierdo AD, Murray EA. Control of response selection by reinforcer value requires interaction of amygdala and orbital prefrontal cortex. J Neurosci. 2000; 20:4311–4319. [PubMed: 10818166]

Beyeler A, Namburi P, Glober GF, Simonnet C, Calhoon GG, Conyers GF, Luck R, Wildes CP, Tye KM. Divergent routing of positive and negative information from the amygdala during memory retrieval. Neuron. 2016; 90:348–361. [PubMed: 27041499]

Britt JP, Benaliouad F, McDevitt RA, Stuber GD, Wise RA, Bonci A. Synaptic and behavioral profile of multiple glutamatergic inputs to the nucleus accumbens. Neuron. 2012; 76:790–803. [PubMed: 23177963]

Burgos-Robles A, Kimchi EY, Izadmehr EM, Porzenheim MJ, Ramos-Guasp WA, Nieh EH, Felix-Ortiz AC, Namburi P, Leppla CA, Presbrey KN, et al. Amygdala inputs to prefrontal cortex guide behavior amid conflicting cues of reward and punishment. Nat Neurosci. 2017; 20:824–835. [PubMed: 28436980]

Cador M, Robbins TW, Everitt BJ. Involvement of the amygdala in stimulus-reward associations: interaction with the ventral striatum. Neuroscience. 1989; 30:77–86. [PubMed: 2664556]

Cardinal RN, Parkinson JA, Hall J, Everitt BJ. Emotion and motivation: the role of the amygdala, ventral striatum, and prefrontal cortex. Neurosci Biobehav Rev. 2002; 26:321–352. [PubMed: 12034134]

Chung K, Wallace J, Kim SY, Kalyanasundaram S, Andalman AS, Davidson TJ, Mirzabekov JJ, Zalocusky KA, Mattis J, Denisin AK, et al. Structural and molecular interrogation of intact biological systems. Nature. 2013; 497:332–337. [PubMed: 23575631]

Ciocchi S, Herry C, Grenier F, Wolff SBE, Letzkus JJ, Vlachos I, Ehrlich I, Sprengel R, Deisseroth K, Stadler MB, et al. Encoding of conditioned fear in central amygdala inhibitory circuits. Nature. 2010; 468:277–282. [PubMed: 21068837]

Corbit LH, Balleine BW. Double dissociation of basolateral and central amygdala lesions on the general and outcome-specific forms of pavlovian-instrumental transfer. J Neurosci. 2005; 25:962–970. [PubMed: 15673677]

Davis M, Shi C. The extended amygdala: are the central nucleus of the amygdala and the bed nucleus of the stria terminalis differentially involved in fear versus anxiety? Ann N Y Acad Sci. 1999; 877:281–291. [PubMed: 10415655]

Do-Monte FH, Minier-Toribio A, Quiñones-Laracuente K, Medina-Colón EM, Quirk GJ. Thalamic regulation of sucrose seeking during unexpected reward omission. Neuron. 2017; 94:388–400. [PubMed: 28426970]

Duvarci S, Pare D. Amygdala microcircuits controlling learned fear. Neuron. 2014; 82:966–980. [PubMed: 24908482]

Fadok JP, Krabbe S, Markovic M, Courtin J, Xu C, Massi L, Botta P, Bylund K, Müller C, Kovacevic A, et al. A competitive inhibitory circuit for selection of active and passive fear responses. Nature. 2017; 542:96–100. [PubMed: 28117439]

Fanselow MS, Kim JJ. Acquisition of contextual Pavlovian fear conditioning is blocked by application of an NMDA receptor antagonist D,L-2-amino-5-phosphonovaleric acid to the basolateral amygdala. Behav Neurosci. 1994; 108:210–212. [PubMed: 7910746]

Felix-Ortiz AC, Tye KM. Amygdala inputs to the ventral hippocampus bidirectionally modulate social behavior. J Neurosci. 2014; 34:586–595. [PubMed: 24403157]

Felix-Ortiz AC, Beyeler A, Seo C, Leppla CA, Wildes CP, Tye KM. BLA to vHPC inputs modulate anxiety-related behaviors. Neuron. 2013; 79:658–664. [PubMed: 23972595]

Felix-Ortiz AC, Burgos-Robles A, Bhagat ND, Leppla CA, Tye KM. Bidirectional modulation of anxiety-related and social behaviors by amygdala projections to the medial prefrontal cortex. Neuroscience. 2016; 321:197–209. [PubMed: 26204817]

Fuster JM, Uyeda AA. Reactivity of limbic neurons of the monkey to appetitive and aversive signals. Electroencephalogr Clin Neurophysiol. 1971; 30:281–293. [PubMed: 4103500]

Goosens KA, Maren S. Contextual and auditory fear conditioning are mediated by the lateral, basal, and central amygdaloid nuclei in rats. Learn Mem. 2001; 8:148–155. [PubMed: 11390634]

Gore F, Schwartz EC, Brangers BC, Aladi S, Stujenske JM, Likhtik E, Russo MJ, Gordon JA, Salzman CD, Axel R. Neural representations of unconditioned stimuli in basolateral amygdala mediate innate and learned responses. Cell. 2015; 162:134–145. [PubMed: 26140594]

Grabenhorst F, Hernádi I, Schultz W. Prediction of economic choice by primate amygdala neurons. Proc Natl Acad Sci USA. 2012; 109:18950–18955. [PubMed: 23112182]

Haight JL, Fuller ZL, Fraser KM, Flagel SB. A food-predictive cue attributed with incentive salience engages subcortical afferents and efferents of the paraventricular nucleus of the thalamus. Neuroscience. 2017; 340:135–152. [PubMed: 27793779]

Hall J, Parkinson JA, Connor TM, Dickinson A, Everitt BJ. Involvement of the central nucleus of the amygdala and nucleus accumbens core in mediating Pavlovian influences on instrumental behaviour. Eur J Neurosci. 2001; 13:1984–1992. [PubMed: 11403692]

Han W, Tellez LA, Rangel MJ Jr, Motta SC, Zhang X, Perez IO, Canteras NS, Shammah-Lagnado SJ, van den Pol AN, de Araujo IE. Integrated control of predatory hunting by the central nucleus of the amygdala. Cell. 2017; 168:311–324. [PubMed: 28086095]

Haubensak W, Kunwar PS, Cai H, Ciocchi S, Wall NR, Ponnusamy R, Biag J, Dong HW, Deisseroth K, Callaway EM, et al. Genetic dissection of an amygdala microcircuit that gates conditioned fear. Nature. 2010; 468:270–276. [PubMed: 21068836]

Holland PC, Gallagher M. Double dissociation of the effects of lesions of basolateral and central amygdala on conditioned stimulus-potentiated feeding and Pavlovian-instrumental transfer. Eur J Neurosci. 2003; 17:1680–1694. [PubMed: 12752386]

Janak PH, Tye KM. From circuits to behaviour in the amygdala. Nature. 2015; 517:284–292. [PubMed: 25592533]

Jimenez SA, Maren S. Nuclear disconnection within the amygdala reveals a direct pathway to fear. Learn Mem. 2009; 16:766–768. [PubMed: 19933881]

Kim J, Pignatelli M, Xu S, Itohara S, Tonegawa S. Antagonistic negative and positive neurons of the basolateral amygdala. Nat Neurosci. 2016; 19:1636–1646. [PubMed: 27749826]

Kim J, Zhang X, Muralidhar S, LeBlanc SA, Tonegawa S. Basolateral to central amygdala neural circuits for appetitive behaviors. Neuron. 2017; 93:1464–1479. [PubMed: 28334609]

Kremer EJ, Boutin S, Chillon M, Danos O. Canine adenovirus vectors: an alternative for adenovirus-mediated gene transfer. J Virol. 2000; 74:505–512. [PubMed: 10590140]

Krettek JE, Price JL. A description of the amygdaloid complex in the rat and cat with observations on intra-amygdaloid axonal connections. J Comp Neurol. 1978; 178:255–280. [PubMed: 627626]

LeDoux JE, Cicchetti P, Xagoraris A, Romanski LM. The lateral amygdaloid nucleus: sensory interface of the amygdala in fear conditioning. J Neurosci. 1990; 10:1062–1069. [PubMed: 2329367]

Lee SC, Amir A, Haufler D, Pare D. Differential recruitment of competing valence-related amygdala networks during anxiety. Neuron. 2017; 96:81–88. [PubMed: 28957678]

Lein ES, Hawrylycz MJ, Ao N, Ayres M, Bensinger A, Bernard A, Boe AF, Boguski MS, Brockway KS, Byrnes EJ, et al. Genome-wide atlas of gene expression in the adult mouse brain. Nature. 2007; 445:168–176. [PubMed: 17151600]

Li H, Penzo MA, Taniguchi H, Kopec CD, Huang ZJ, Li B. Experience-dependent modification of a central amygdala fear circuit. Nat Neurosci. 2013; 16:332–339. [PubMed: 23354330]

Livneh Y, Ramesh RN, Burgess CR, Levandowski KM, Madara JC, Fenselau H, Goldey GJ, Diaz VE, Jikomes N, Resch JM, et al. Homeostatic circuits selectively gate food cue responses in insular cortex. Nature. 2017; 546:611–616. [PubMed: 28614299]

Maren S, Quirk GJ. Neuronal signalling of fear memory. Nat Rev Neurosci. 2004; 5:844–852. [PubMed: 15496862]

Miserendino MJD, Sananes CB, Melia KR, Davis M. Blocking of acquisition but not expression of conditioned fear-potentiated startle by NMDA antagonists in the amygdala. Nature. 1990; 345:716–718. [PubMed: 1972778]

Namburi P, Beyeler A, Yorozu S, Calhoon GG, Halbert SA, Wichmann R, Holden SS, Mertens KL, Anahtar M, Felix-Ortiz AC, et al. A circuit mechanism for differentiating positive and negative associations. Nature. 2015; 520:675–678. [PubMed: 25925480]

Namburi P, Al-Hasani R, Calhoon GG, Bruchas MR, Tye KM. Architectural representation of valence in the limbic system. Neuropsychopharmacology. 2016; 41:1697–1715. [PubMed: 26647973]

Paton JJ, Belova MA, Morrison SE, Salzman CD. The primate amygdala represents the positive and negative value of visual stimuli during learning. Nature. 2006; 439:865–870. [PubMed: 16482160]

Paxinos, G., Franklin, KBJ. The Mouse Brain in Stereotaxic Coordinates. Gulf Professional Publishing; 2004.

Penzo MA, Robert V, Li B. Fear conditioning potentiates synaptic transmission onto long-range projection neurons in the lateral subdivision of central amygdala. J Neurosci. 2014; 34:2432–2437. [PubMed: 24523533]

Ramirez S, Liu X, MacDonald CJ, Moffa A, Zhou J, Redondo RL, Tonegawa S. Activating positive memory engrams suppresses depression-like behaviour. Nature. 2015; 522:335–339. [PubMed: 26085274]

Redondo RL, Kim J, Arons AL, Ramirez S, Liu X, Tonegawa S. Bidirectional switch of the valence associated with a hippocampal contextual memory engram. Nature. 2014; 513:426–430. [PubMed: 25162525]

Sanford CA, Soden ME, Baird MA, Miller SM, Schulkin J, Palmiter RD, Clark M, Zweifel LS. A central amygdala CRF circuit facilitates learning about weak threats. Neuron. 2017; 93:164–178. [PubMed: 28017470]

Schoenbaum G, Chiba AA, Gallagher M. Neural encoding in orbitofrontal cortex and basolateral amygdala during olfactory discrimination learning. J Neurosci. 1999; 19:1876–1884. [PubMed: 10024371]

Shabel SJ, Janak PH. Substantial similarity in amygdala neuronal activity during conditioned appetitive and aversive emotional arousal. Proc Natl Acad Sci USA. 2009; 106:15031–15036. [PubMed: 19706473]

Stuber GD, Sparta DR, Stamatakis AM, van Leeuwen WA, Hardjoprajitno JE, Cho S, Tye KM, Kempadoo KA, Zhang F, Deisseroth K, Bonci A. Excitatory transmission from the amygdala to nucleus accumbens facilitates reward seeking. Nature. 2011; 475:377–380. [PubMed: 21716290]

Tye KM, Stuber GD, de Ridder B, Bonci A, Janak PH. Rapid strengthening of thalamo-amygdala synapses mediates cue-reward learning. Nature. 2008; 453:1253–1257. [PubMed: 18469802]

Tye KM, Prakash R, Kim SY, Fenno LE, Grosenick L, Zarabi H, Thompson KR, Gradinaru V, Ramakrishnan C, Deisseroth K. Amygdala circuitry mediating reversible and bidirectional control of anxiety. Nature. 2011; 471:358–362. [PubMed: 21389985]

Viviani D, Charlet A, van den Burg E, Robinet C, Hurni N, Abatis M, Magara F, Stoop R. Oxytocin selectively gates fear responses through distinct outputs from the central amygdala. Science. 2011; 333:104–107. [PubMed: 21719680]

Wilensky AE, Schafe GE, LeDoux JE. Functional inactivation of the amygdala before but not after auditory fear conditioning prevents memory formation. J Neurosci. 1999; 19:RC48. [PubMed: 10594092]

Zhang W, Schneider DM, Belova MA, Morrison SE, Paton JJ, Salzman CD. Functional circuits and anatomical distribution of response properties in the primate amygdala. J Neurosci. 2013; 33:722–733. [PubMed: 23303950]

Highlights

- BLA neurons projecting to NAc, CeA, and vHPC are intermingled in distinct gradients
- Positive and negative valence-encoding BLA neurons are intermingled throughout BLA
- Projection-defined BLA populations differ in the size of local networks recruited
- BLA-CeA neurons suppress a larger local network than BLA-NAc or BLA-vHPC neurons

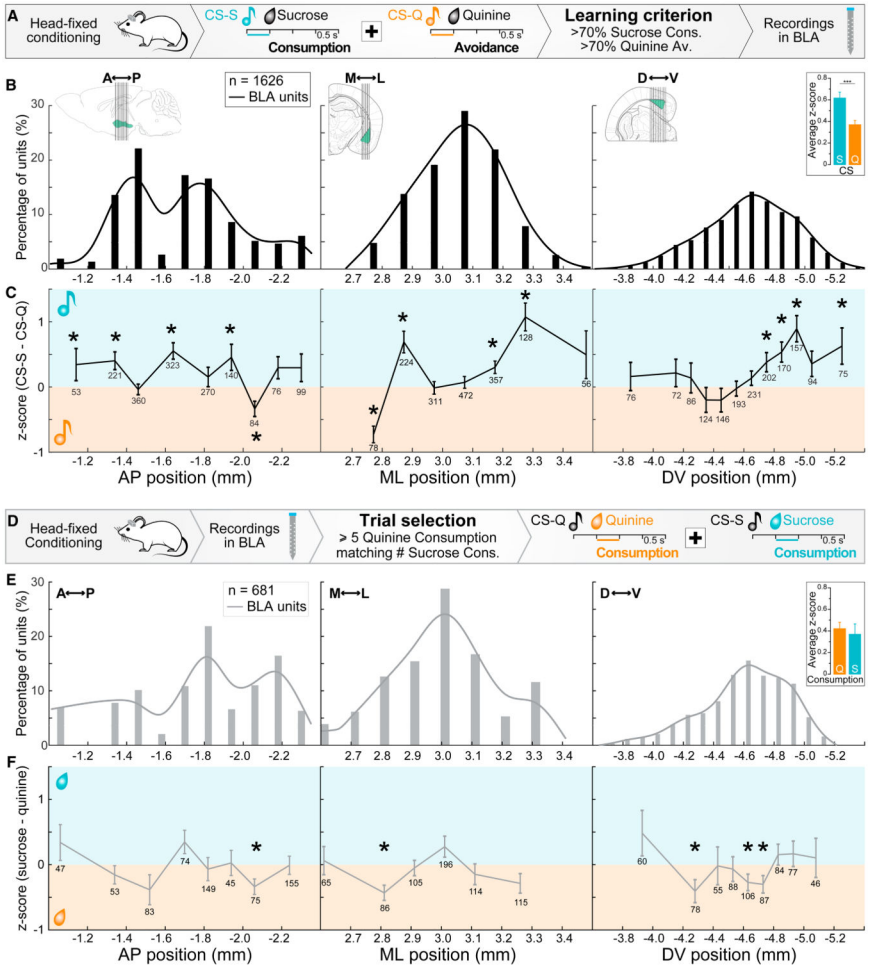

Figure 1. Mapping BLA Neuron Response to CSs and USs of Positive and Negative Valence

(A) Schematic of the Pavlovian conditioning paradigm. Head-fixed mice were trained to discriminate between one cue paired with the presentation of sucrose (CS-S) and a second cue paired with quinine (CS-Q). After reaching the learning criterion, acute single-unit recordings were performed in the BLA.

(B) Distribution of neurons recorded in the basolateral amygdala (BLA) in the anteroposterior (AP), mediolateral (ML), and dorsoventral (DV) axes, expressed as the percentage of all recorded units and fitted with a spline interpolation. Inset on the right: the average Z score across all units is higher during the CS-S compared to the CS-Q (paired t test, t = 4.872, ***p < 0.001, n = 1,626).

(C) Differential Z score for all recorded units between the CS-S (before sucrose delivery, blue line in A) and the CS-Q (before the quinine delivery, orange line in A) depending on AP, ML, and DV location. Numbers indicate the number of units sampled at each coordinate. Paired t tests indicate when responses were significantly higher for the CS-S or CS-Q (*p < 0.05).

(D) After head-fixed conditioning up to the learning criterion and recording, units recorded during at least 5 quinine consumptions (error trials) were selected, and the responses to the

quinine consumptions (Z score during orange line) and to a matching number of sucrose consumptions (Z score during blue line) were compared.

(E) Distribution of neurons recorded in the AP, ML, and DV axes of the BLA, expressed as the percentage of all units recorded during at least 5 quinine consumptions. The distribution is fitted with a spline interpolation. Inset on the right: the average Z score across all units is similar between sucrose and quinine consumptions (paired t test, $t = 0.749$, $p = 0.450$, $n = 681$).

(F) Differential Z score of units recorded during at least 5 quinine consumptions in the AP, ML, and DV axes of the BLA. Paired t tests indicated positions wherein the average Z score for the response to quinine was greater than that for sucrose (*$p < 0.05$).

Error bars represent the SEM.

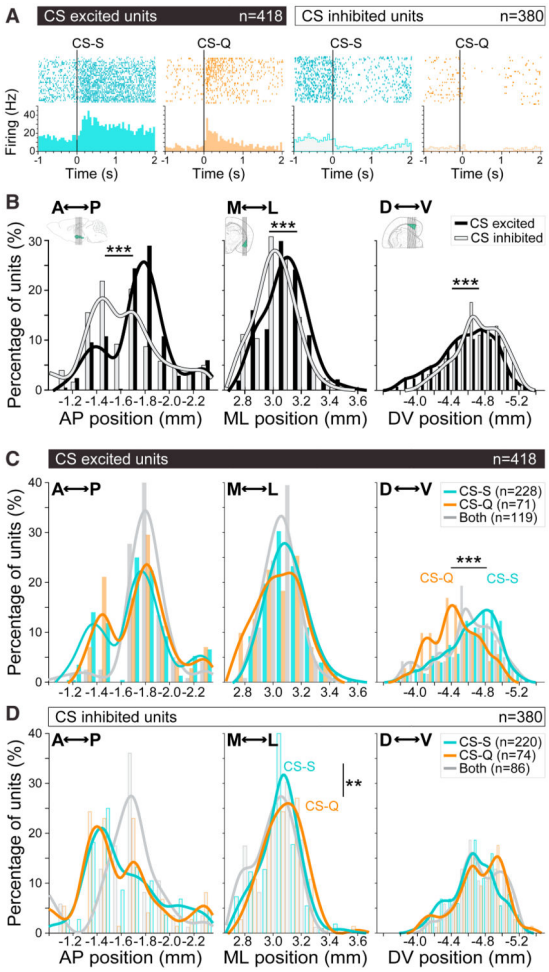

Figure 2. Mapping BLA Neurons Excited and Inhibited to Positive and Negative CS

(A) Peri-event rasters and Peristimulus Time Histograms of the firing rates of four representative units recorded in the BLA.

(B) Distribution in AP, ML, and DV dimensions of the units excited to at least one CS (black, increased firing with signed rank-sum test, $p < 0.01$) and of units inhibited to at least one CS (gray, decrease firing with signed rank-sum test, $p < 0.01$). The proportion is expressed as a percentage of all excited units (black bars, n = 418) or all inhibited units (gray bars, n = 380). Units excited to the CS are more posterior (rank-sum test, ***$p < 0.001$), more lateral (rank-sum test, **$p < 0.01$), and more dorsal (rank-sum test, ***$p < 0.001$) compared to units inhibited to the CS. The histograms are fitted with a spline interpolation. Units responding to both cues in an opposite direction were excluded (n = 12).

(C) Fraction of BLA units excited (increased firing with signed rank-sum test, $p<0.01$) in response to the CS-S (blue), the CS-Q (orange), or both cues (gray) at different coordinates in the AP, ML, and DV dimensions of the BLA. The fraction is expressed as a percentage of all units excited to the CS-S (n = 228), to the CS-Q (n = 71), or to both cues (n = 119). The distribution is significantly different between the CS-S and the CS-Q in the DV dimension (rank-sum test, ***$p<0.001$), with a larger proportion of neurons excited to the CS-Q in the dorsal BLA and a larger proportion of units excited to the CS-S in the ventral BLA.

(D) Distribution of the units inhibited (decreased firing with signed rank-sum test, $p < 0.01$) in response to the CS-S (blue), the CS-Q (orange), or both cues (gray) in the AP, ML, and DV axes of the BLA. The proportion at each coordinate is expressed as a percentage of all units inhibited to the CS-S (n = 220), to the CS-Q (n = 74), or to both cues (n = 119). The distribution is significantly different between the CS-S and the CS-Q in the ML dimension (rank-sum test, $^{**}p < 0.01$), with a larger proportion of neurons inhibited to the CS-S than in the CS-Q at the center of the ML dimension.

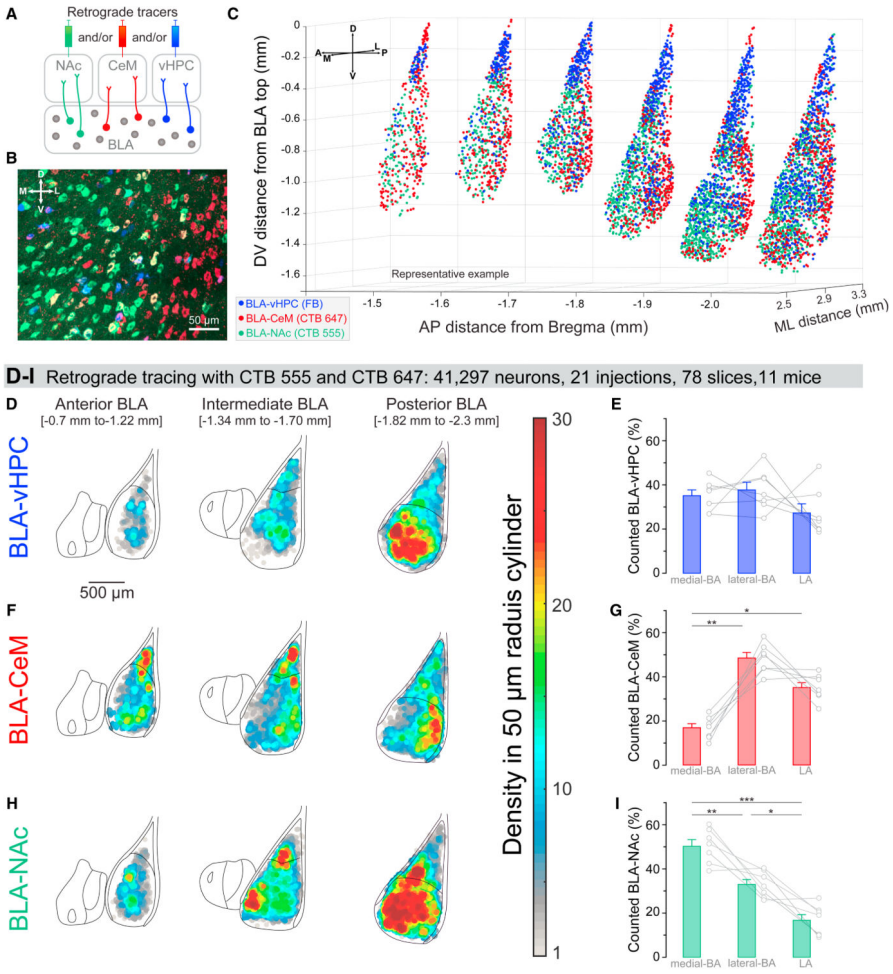

Figure 3. Localization of BLA Projectors

(A) Retrograde fluorescent tracers were injected in the ventral hippocampus (vHPC), the centromedial nucleus of the amygdala (CeM), and/or the nucleus accumbens (NAc).

(B) Confocal image of BLA neurons projecting to the vHPC (BLA-vHPC, blue), to the CeM (BLA-CeM, red), and to the NAc (BLA-NAc, green) in one representative animal injected with fast blue in the vHPC, CTB 647 in the CeM, and CTB 555 in the NAc. M, medial; L, lateral; D, dorsal; V, ventral.

(C) 3-dimensional plot of the animal showed in (B). Each cluster of dots represents BLA projectors quantified in one section in the AP dimension of the BLA. A, anterior; P, posterior.

(D–I) Heatmaps of the density of the three types of projectors labeled with the CTB tracers (CTB 555 or CTB 647) (D, F, and H). The density was computed for each neuron in a 50 µm cylinder of a 50 µm depth and then color coded and superimposed across animals depending on the categories of the AP coordinate (anterior, intermediate, and posterior). n = 11 mice, (7 mice per injection site), 78 slices, 41,297 neurons. Percentages of BLA-vHPC, BLA-CeM, and BLA-NAc projectors counted in the lateral amygdala (LA), the medial BA, and the lateral BA (E, G, and I). Each gray circle next to a bar reflects the percentage of projectors in

one mouse. (E) BLA-vHPC projectors are equally distributed in the LA, the medial BA, and the lateral BA (one-way ANOVA, $F_{(1.62, 9.72)} = 1.61$, $p > 0.05$).
(G) BLA-CeM projectors are located significantly more in the LA and in the lateral BA (one-way ANOVA, $F_{(1.85, 11.07)} = 33.23$, $p < 0.001$; Tukey's multiple comparisons of medial BA versus lateral BA, $^{**}p < 0.01$, and medial BA versus LA, $^{*}p < 0.05$).
(I) BLA-NAc projectors are mainly present in the medial BLA and are denser in the lateral BLA compared to the LA (one-way ANOVA, $F_{(1.82, 10.94)} = 27.52$, $p < 0.001$; Tukey's multiple comparisons of medial BA versus lateral BA, $^{**}p < 0.01$; medial BA versus LA, $^{***}p < 0.001$; and lateral BA versus LA, $^{*}p < 0.05$).
Error bars represent the SEM.

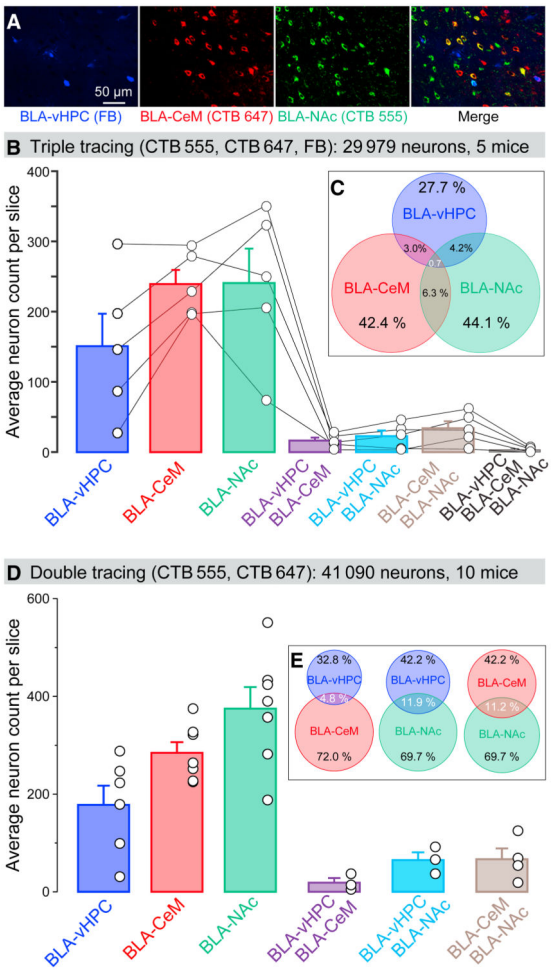

Figure 4. Overlap of Retrograde Tracers in BLA Neurons

(A) Confocal image within the BLA of a mouse that received three tracer injections: FB in vHPC (blue), CTB 647 in CeM (pseudocolored in red), and CTB 555 in NAc (pseudocolored in green).

(B) Average number of projectors counted per slice in each mouse that received three tracer injections (one fast blue and two CTB).

(C) Venn diagram illustrating the percentage of neurons containing one, two, or three tracers and therefore projecting to one, two, or three of the injected downstream targets.

(D) Average number of projectors counted per slice in each mouse that received two CTB injections.

(E) Venn diagrams representing the percentage of neurons containing one or two CTB tracers and therefore projecting to one or two of the injected downstream targets.

Error bars represent the SEM.

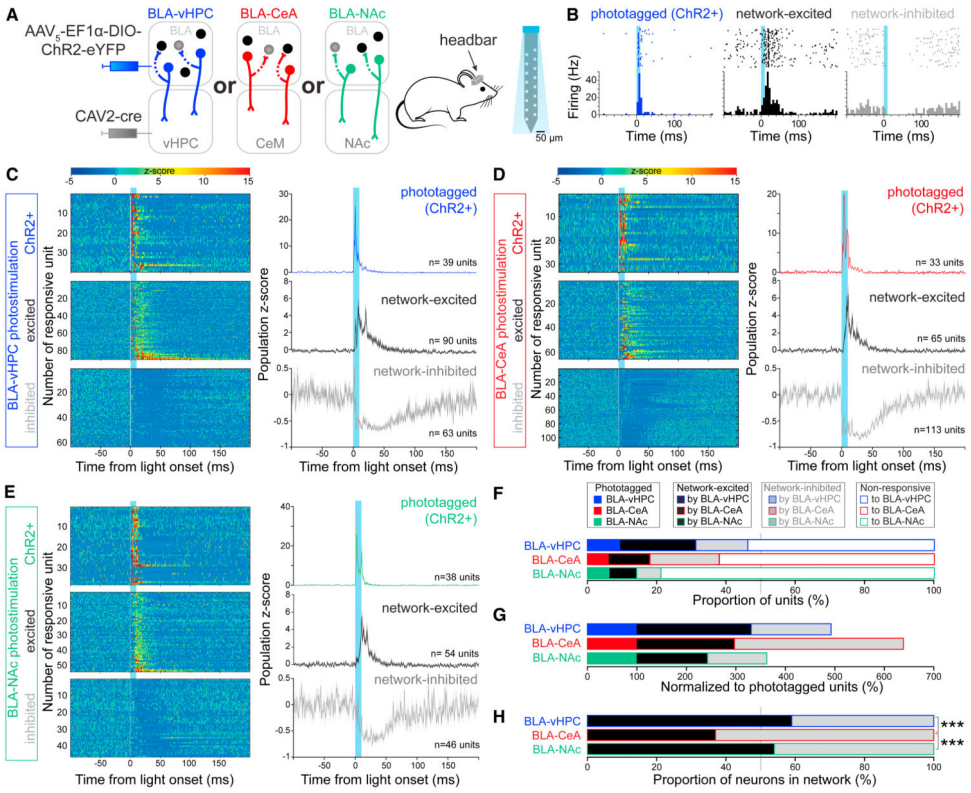

Figure 5. Influence of BLA Projector Photostimulation on BLA Single Units

(A) Dual-vector recombination was used to express ChR2-eYFP in BLA-vHPC, BLA-CeA, and BLA-NAc projectors before recording single units in the BLA of awake, head-fixed mice using 16 channel silicon optrodes.

(B) Raster plot of action potential and peri-event stimulus histogram of the firing rate of one unit identified as a BLA-vHPC phototagged neuron (phototagged, left panel, blue; defined by an increase in firing; the signed rank-sum test, $p < 0.01$; and a response latency < 6 ms), another unit excited but with a photo-response latency greater than the patch-clamp validated threshold (network-excited, middle panel, black; defined by an increase in firing but with a response latency > 6 ms), and a unit inhibited by projector activation (network-inhibited, right panel, gray; defined by decreased firing).

(C) Color-coded plot of the Z score of every unit within each phototagged (top), network-excited (middle), and network-inhibited (bottom) population in response to a 10 ms blue light pulse within animals expressing ChR2 in BLA-vHPC projectors. Right: the average Z score of these 3 subpopulations (±SD).

(D) Color-coded plot of the Z score of every unit within each phototagged (top), network-excited (middle), and network-inhibited (bottom) population in response to a 10 ms blue light pulse within animals expressing ChR2 in BLA-CeA projectors. Right: the average Z score of these 3 subpopulations (±SD).

(E) Color-coded plot of the Z score of every unit within each phototagged (top), network-excited (middle), and network-inhibited (bottom) population in response to a 10 ms blue light pulse within animals expressing ChR2 in BLA-NAc projectors. Right: the average Z score of these 3 subpopulations (±SD).

(F) Proportion of BLA units responding to the photostimulation of BLA-vHPC projectors (blue, top row), BLA-CeA projectors (red, middle row), and BLA-NAc projectors (green, bottom row) with an excitatory response (projectors and units excited by projector photostimulation) or an inhibitory response (units inhibited by projector photostimulation).
(G) Proportion of network-excited and network-inhibited units normalized by the number of phototagged BLA-vHPC projectors (blue, top row, n = 39), BLA-CeA projectors (red, middle row, n = 33), and BLA-NAc projectors (green, bottom row, n = 38).
(H) Photostimulation of BLA-vHPC projectors (blue, top row) and BLA-NAc projectors (green, bottom row) excites significantly more units compared to the photostimulation of BLA-CeA projectors (red, middle row), which inhibits more cells (binomial test, ***$p < 0.001$, corrected for multiple comparisons).

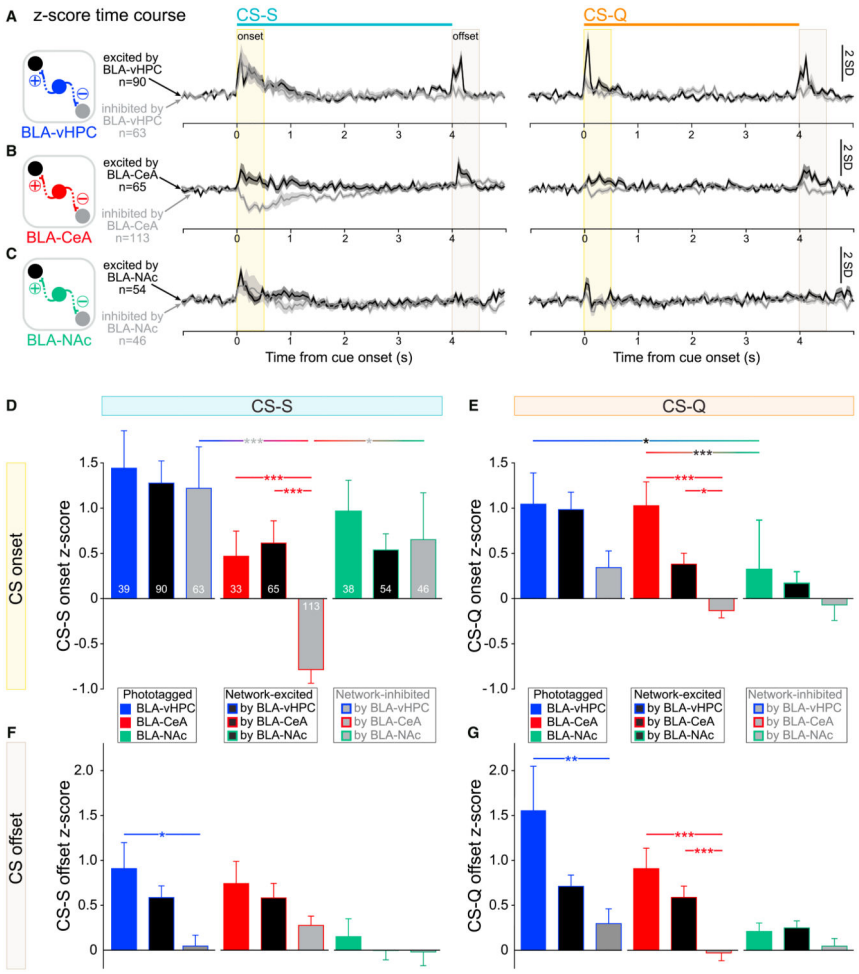

Figure 6. Valence Coding Properties of BLA Projector Microcircuits

(A) The time courses of the *Z* score of BLA neurons excited (black) or inhibited (gray) by the photostimulation of BLA-vHPC projectors shows an excitatory response to the onset of the CS-S (blue line, left panel) and to the onset of the CS-Q (orange line, right panel).

(B) BLA neurons network-excited by the photostimulation of BLA-CeA projectors (black) have a transient excitatory response to the onset of the CS-S and CS-Q, while units network-inhibited by the photostimulation of BLA-CeA projectors (gray) display inhibitory responses to the onset of the CS-S and CS-Q.

(C) Time courses of the *Z* score of BLA neurons excited (black) or inhibited (gray) by the photostimulation of BLA-NAc projectors show an excitatory response to the onset of the CS-S and CS-Q.

(D) Average *Z* score in response to the CS-S onset (before sucrose delivery) for units phototagged, network-excited, or network-inhibited by photoactivation of BLA-vHPC (blue), BLA-CeA (red), or BLA-NAc (green) projectors.

(E) Average *Z* score in response to the CS-Q onset (before sucrose delivery) for units phototagged, network-excited, or network-inhibited by photoactivation of BLA-vHPC (blue), BLA-CeA (red), or BLA-NAc (green) projectors.

(F) Average *Z* score in response to the CS-S offset (after CS-S termination) for units phototagged, network-excited, or network-inhibited by photoactivation of BLA-vHPC (blue), BLA-CeA (red), or BLA-NAc (green) projectors.
(G) Average *Z* score in response to the CS-Q offset (after CS-Q termination) for units phototagged, network-excited, or network-inhibited by photoactivation of BLA-vHPC (blue), BLA-CeA (red), or BLA-NAc (green) projectors.
Error bars represent the SEM.